33RD INTERNATIONAL COSMIC RAY CONFERENCE, RIO DE JANEIRO 2013
THE ASTROPARTICLE PHYSICS CONFERENCE

ICRC 2013

Estimated exposure of UHECR observation by the JEM-EUSO mission

K. SHINOZAKI[1], M.E. BERTAINA [2], S. BIKTEMEROVA[3], P. BOBIK[4], F. FENU[1,5], A. GÚZMAN[1], F. GUARINO[6], G. MEDINA TANCO[7], T. MERNIK[1], J.A. MORALES DE LOS RIOS PAPPA[8,5], D. NAUMOV[3], G. SAÉZ CÁNO[8], N. SAKAKI[9], A. SANTANGELO[1], S. TOSCANO[10] AND L. VALORE[6] FOR THE JEM-EUSO COLLABORATION

[1]*Institut für Astronomie und Astrophysik, Eberhard Karls Universität Tübingen, Sand 1, 72076 Tübingen, Germany*
[2]*Department of General Physics, University of Torino, Via P. Giuria 1, 10125 Turin, Italy*
[3]*Joint Institute for Nuclear Research, Joliot-Curie 6, 141980 Dubna, Russia*
[4]*Insteitute of Experimental Physics, Slovak Academy of Science, Watsonova 47, 040 01, Kosice, Slovakia*
[5]*Computational Astrophysics Laboratory, RIKEN, 2-1 Hirosawa, Wako 351-0198, Japan*
[6]*Istituto Nazionale di Fisica Nucleare - Sezione di Napoli, via Cintia, 80126 Naples, Italy*
[7]*Instituto de Ciencias Nucleares, Universitat Natcional Autonoma Mexico, Apartado Postal 70-543, Mexico D.F. 04510, Mexico*
[8]*Space and Astroparticles Group, University of Alcala, 28807 Alcala de Henares, Spain*
[9]*Institut für Kernphysik, Kalsruhe Institut fúr Technologie, Hermann-vol-Hlmholtz Plaz 1, 76344 Eggenstein-Lepopldshafen, Germany*
[10]*ISDC Data Centre for Astrophysics, Chemin d'Ecogia 16, 1290 Versoix, Switzerland*

kenjikry@astro.uni-tuebingen.de

Abstract: The nature of the ultra-high energy cosmic rays (UHECRs) remains unsolved mystery mainly due to severely low fluxes for ground-based observatories. The JEM-EUSO (Extreme Universe Space Observatory on-board the Japanese Experiment Module) mission operates huge-aperture UHECR observation via extensive air shower (EAS) observation from the International Space Station. To evaluate the performance in exposure, a large number of EAS simulations are generated taking into account EAS properties, background noise, role of the cloud and the configuration of the JEM-EUSO telescope. The results show that observation to the nadir direction reaches about 9 times annual exposures compared to that is achieved by the largest existing detector. The enhancement of exposure by tilting the telescope is also demonstrated. Operating on the orbit allows the full coverage of the Celestial at high degree of uniformity for the analysis of the UHECR arrival direction distribution.

Keywords: JEM-EUSO, ultra-high energy cosmic rays, space instrument, fluorescence detector

1 Introduction

The nature of the ultra-high energy cosmic rays (UHECRs) remains a long lasting mystery in astrophysics [1]. So far, extremely low fluxes of UHECRs have constrained effective observation and no origin has been identified. In ground-based observatories, the observable region and efficiency in surveying the Celestial Sphere depend on geographical location. Thus, dramatic increases of effective areas with all-sky coverage capability are highly desired in forthcoming era of UHECR physics.

The JEM-EUSO (Extreme Universe Space Observatory on-board the Japanese Experiment Module) mission [2] is a novel approach by fluorescence technique in space to investigate science objectives for UHECRs [3]. In the present work, we aim at estimating the fundamental performance, mainly focusing on the expected exposure of the mission in various operational conditions. The exposure is a basic measure to evaluate the statistics of observed UHECR events. We discuss the key pretties and factors that determine the exposure such as EAS development, condition within the field of view (FOV), detector responses and observation time.

2 Apparatus

The JEM-EUSO observatory is the ensemble of the UV telescope, referred to as 'main telescope,' the atmospheric monitoring (AM) system [4] and other sub-system instruments. It is designed to operate on the JEM *Kibo* module of the International Space Station (ISS) [5]. Orbiting at a nominal altitude $H_0 \sim 400$ km from the Earth's surface (hereafter, meant for an assumed ellipsoid), it revolves every ~ 90 min at sub-satellite speed of ~ 7 km s^{-1}. According to inclination, the ISS operation extends latitudes within $\pm 51.6^\circ$. During the operation, the JEM-EUSO instrument may be pointed to the nadir, referred to as 'nadir mode' or tilted astern, 'tilt mode.'

The main telescope is designed to detect moving tracks of the ultra-violet (UV) photons produced in extensive air showers (EASs). It consists of a 4.5-m^2 Fresnel optics [6] viewed by the focal surface (FS) detector [7]. It is formed by 137 photo-detector modules (PDMs). Each PDM is a set of 36 multi-anode photomultiplier tubes (MAPMTs) with 64 pixels. The effective FOV $\omega_{\rm FOV}$ is ~ 0.85 sr with a spatial resolution of 0.075° equivalent to ~ 0.5 km on the surface. The time resolution is 2.5 μs called gate time unit (GTU). Due to a limited telemetry budget, two levels of trigger algorithms [8] are operated to search every PDM for stationary and transient excesses of EAS signals over prevailing background in the nighttime atmosphere [9]. Threshold levels for trigger criteria are dynamically set to fit permissible fake trigger rates at an order of ~ 0.1 Hz.

3 Observed properties of EAS

In the present work to simulate EAS and detector response, we employ the ESAF (EUSO Simulation and Analysis Framework) package [10] adapted into the JEM-EUSO baseline configuration (see Refs. [7] for details). The

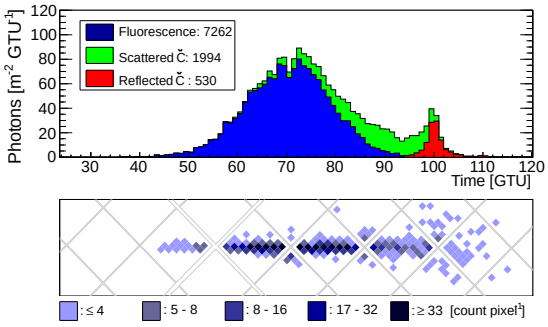

Figure 1: Arrival time distribution of photons (top panel) from a typical EAS of $E_0 = 10^{20}$ eV from $\Theta = 60^\circ$ and time-integrated signals on the FS detector (bottom). In the top panel, components of fluorescence photons, and scattered and reflected Cherenkov photons are shown by different histograms. In the bottom panel, signal counts per pixel are indicated by filled squared. The gray lines denote the MAPMT boundaries. The horizontal position along the EAS axis corresponds to the arrival time on the top panel.

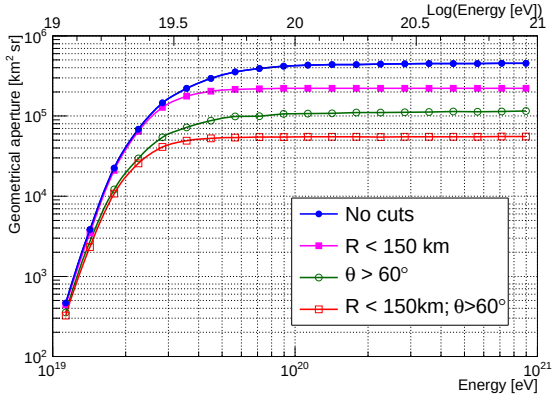

Figure 2: Geometrical aperture as a function of energy. Closed circles show the case without cuts. Closed squares and open circles indicate for the cuts of $R < 150$ km and $\Theta > 60^\circ$. Open squares are for the combined case.

altitude of JEM-EUSO is set to be 400 km for the nadir mode and the case of 350 km is also tested. The tilt mode cases are also investigated for relevant interests. The clear atmosphere condition is assumed in the simulation. The role of clouds and the influence on the exposure are separately taken into account[11]. As a nominal assumption, the background level from night glow in the dark night I_{BG} is set to 500 photons m^{-2} sr^{-1} ns^{-1} [9].

In Figure 1, the top panel shows the arrival time distribution of photons from a typical EAS. Fluorescence and scattered and reflected Cherenkov light components are shown by the different histograms. The sample is the case for an EAS of energy $E = 10^{20}$ eV from zenith angle $\Theta = 60^\circ$. The horizontal axis denotes the absolute time and is set 100 GTUs at the time that shower particles on the axis reach the surface level. The bottom panel displays the time-integrated image of signals on the FS detector. Signal counts per pixel are indicated by the filled squares with MAPMT boundaries shown by gray lines. The horizontal position corresponds to the arrival time on the top panel.

In UHECR observation from space, fluorescence light is the dominant component of signals and its luminosity is almost proportional to the energy deposited by the EAS particles. A part of Cherenkov light that is scattered in the atmosphere is also observed. In addition, the space-based observation also detects the reflection of Cherenkov photons from land or water as well as cloud. Those reflection signals, referred to as 'Cherenkov footprint,' provide a piece of information on the position and timing of the EAS reaching such boundaries.

For EASs of a given energy, intrinsic observable properties are dominantly determined by the zenith angle of EASs. For larger zenith angles, EASs result in signals more intense with longer apparent track and duration. These effects are all in favor to the trigger algorithms as well as subsequent event reconstruction. Within FOV of the main telescope, the vignetting of the optics depends on the direction of EASs with respect to the optical axis. Also the EASs in the direction of FOV edge is more distant and the overall effect reduces the signal intensity [11].

4 Geometrical aperture

To estimate the geometrical aperture, a large number of EASs are simulated over a far larger area than that seen by optics, namely $\omega_{\rm FOV} \cdot {H_0}^2 \sim 1.4 \times 10^5$ km^2 for $H_0 = 400$ km. The geometrical aperture $A(E)$ is wwritten as a function of energy E by the product of simulated area, solid angle acceptance and probability of trigger obtained by simulations. Simple geometrical cuts may be applied on displacement R of the impact location of the EAS from the projected center of the FOV on surface and on the lower limit of zenith angles $\Theta_{\rm cut}$. The subsection of the aperture for such cuts is given in the same way for an area of πR^2 and a solid angle acceptance of $\pi \cdot \cos^2\Theta_{\rm cut}$ [sr]. The latter is a result of an integral of solid angle element weighted by projected area from EAS point of view. These cuts are used to select the events with larger signals. Unlike ground-based observatories, the spaced-based ones are more sensitive to larger zenith angle EASs.

Figure 2 shows the geometrical aperture as a function of energy for $H_0 = 400$ km without geometrical cuts (closed circles) a cut of $R < 150$ km (closed squares), of $\theta < 60^\circ$-cut (open circles) and their combination (open squares).

The geometrical aperture without cut reaches the plateau around $(6-7) \times 10^{19}$ eV. From the FOV of the optics, the saturated aperture is $\sim 4.3 \times 10^5$ km^2 sr. Slight increase seen at the highest energies is due to a little contribution by the EASs part of which cross the FOV. Applying the geometrical cuts helps lower the energy where the aperture saturates. With both $R < 150$ km and $\Theta > 60^\circ$ cuts, though it reduces the saturated aperture to be about an eighth of that without cuts, a constant aperture is achieved at $\sim 3 \times 10^{19}$ eV. Extension of plateau region towards lower energies allows a cross-check of the flux measured by the full sample of events in the specific range of energies. Consequently, the overlapping energy range between JEM-EUSO and ground-based observatories is enlarged.

Results shown above are for the case of $H_0 = 400$ km. Among the orbital elements of the ISS, the altitude H_0 varies throughout the time and is not predictable for the era of the mission. As the observation area in the nadir mode is scaled by ${H_0}^2$, operation at lower altitudes correspondingly lessens the saturated aperture. In the tilt mode, however,

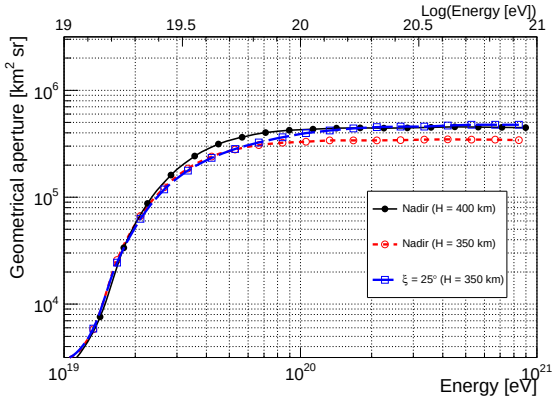

Figure 3: Aperture as a function of energy for the nadir mode at $H_0 = 400$ km (closed circles) and 350 km (open circles) as well as one for a quasi-nadir mode with $\xi = 25^\circ$ at $H_0 = 350$ km (open squares).

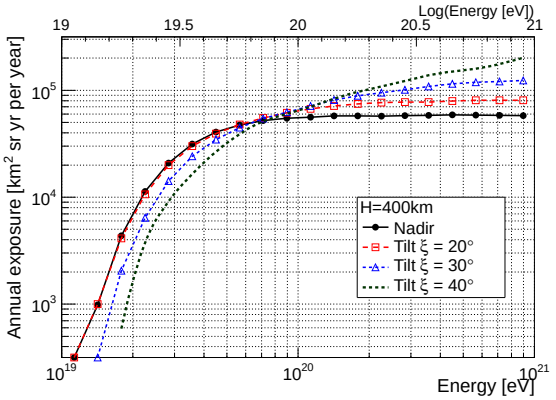

Figure 4: Annual exposure as a function of energy for nadir mode (closed circles) and tilt modes for $\xi = 20^\circ$ (open squares) and 30° (open triangle). The case for $\xi = 40^\circ$ is shown as a reference. $H_0 = 400$ km is assumed.

tilting the telescope increases the projected area of FOV on the Earth's surface. With tilting angle $\xi \lesssim 30^\circ$, it grows proportional to $\sim (\cos\xi)^{-3}$. This allows recovery of observation areas in lower altitude operation. In even larger tilting angles, the effect of the Earth's curvature further amplifies this factor. At $H_0 = 400$ km, the projected observation area for $\xi \sim 40^\circ$ where the edge of FOV does not see the sky above the local horizon reaches ~ 6 times of that of the nadir mode.

In Figure 3, the apertures as a function of energy are shown for nadir mode at $H_0 = 400$ km (closed circles) and 350 km (open circles). For the latter, the case for $\xi = 25^\circ$ is also indicated by the open squares.

In this example of $H_0 = 350$ km, the saturated aperture decreases by ~ 30 % in comparison to the case of $H_0 = 400$ km. Note that in this case the threshold in energy lowers by the same factor as the distance to EAS is closer. Also by tilting the telescope by $\sim 25^\circ$, referred to as 'quasi-nadir mode,' the saturated aperture is similar to that of nadir mode at $H_0 = 400$ km.

5 Exposure

In order to estimate the number of events observed by the JEM-EUSO mission, the exposure growth per unit time such as one-year operation is an essential measure. Apart from the nominal geometrical aperture, reduction factors in exposure and observation on-time should be taken in account. In the present work, the exposure per year of operation for events that trigger JEM-EUSO, defined as the 'annual exposure' is evaluated as follows:

$$(\text{Annual exposure}) \equiv A(E) \cdot \kappa_C \cdot \eta_0 \cdot (1 - f_{\text{loc}}) \cdot (1\ \text{yr}), \quad (1)$$

where $\kappa_C \approx 0.72$ is a cloud efficiency, $\eta_0 \approx 0.2$ is an observational duty cycle and $f_{\text{loc}} \approx 0.1$ is the fraction of locally light-polluted areas. The details of those factors have been intensively investigated in Ref. [11]. The cloud efficiency is defined as the ratio in trigger aperture between the cases with and without cloud coverage taken into account. In this estimation, the visibility of the EAS maximum above or through the cloud is required. The observational duty cycle is the fraction of time in which the background level I_{BG} is below a given threshold level. Here $I_{\text{BG}} < 1500$ photons m^{-2} sr^{-1} ns^{-1} is assumed to suppress high back-scattered moonlight. Note that it does not limit the operation of the main telescope and is conservative for EASs at highest energies. The factor for the local light coverages applies to man-made light such as cities. The reduction by the occurrence of aurorae is also included.

The exposure for tilt mode is also evaluated. As discussed in the previous section, the observation area increases in the tilt mode, while the observable time may be reduced since both the ISS and the region within FOV should be in Earth's umbra. In the present work, we deliver as first results based on the direct application of Eq. (1).

Figure 4 shows the annual exposures at $H_0 = 400$ km as a function of energy for the nadir mode (closed circles) and tilt modes for $\xi = 20^\circ$ (open squares) and 30° (open triangle). The case for $\xi = 40^\circ$ is shown as a reference.

According to Eq. (1), the conversion factor between exposure and geometrical apertures ~ 0.13 yr. The operational inefficiencies due to the events such as rocket docking, lid operation, detector maintenance or aging, etc. as well as quality cuts on reconstruction are not yet taken into account. The latest results on the reconstruction are addressed in Ref. [12]. Therefore, the present results constitute an upper limit on the effective exposure of the instrument for the assumed conditions.

In the case of the nadir mode, the annual exposure at saturated level is expected to be ~ 9 times greater than that of the Pierre Auger Observatory with the corresponding value of about 7000 km^2 sr yr [13]. Because of the steeply rising aperture at lower energies, the subsets of data with reduced but flat exposure are used down to $\sim (2-3) \times 10^{19}$ eV to cross-check with measurements by other ground-based experiments. It is important to underline that the most stringent cuts shown in Figure 2 correspond to an annual exposure comparable to that of Auger even at $\sim 3 \times 10^{19}$ eV. This means that statistically similar data samples are obtained. In this way, it allows to have a comparison of UHECR fluxes for one entire energy-decade above this energy.

The quasi-nadir mode such as $\xi = 20^\circ$ case allows to slightly increase the exposure above 10^{20} eV. This is an interesting option to recover the exposure from unexpected

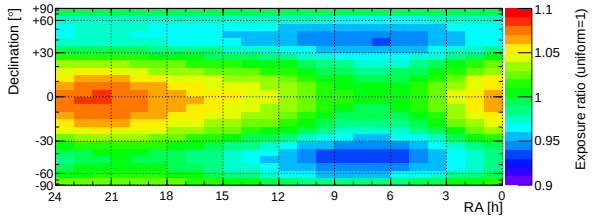

Figure 5: Relative exposure as a function of declination and right ascension in color scale. The impact of cloud coverage is investigated from TOVS database [14]. The nadir mode is assumed for this analysis.

operational inefficiencies. In the tilt mode at $\xi = 30^\circ$, the increase of exposure is a factor of ~ 2 at $\sim 3 \times 10^{20}$ eV.

So far, a constant background level has been assumed, while it is variable with time. By increasing the maximum acceptable background level, the observational time increases as well. The trigger system is capable of dynamically adjusting the thresholds to cope with variable background intensity [8]. The exposure function shifts in energy proportional to $\sim \sqrt{I_{\rm BG}}$ as it depends on Poissonian fluctuations of the average background level. Along with possible tilt mode operation, this is particularly useful to explore the extreme energy ranges with elongated exposures.

In the end, it is also interesting to mention that unlike ground-based observatories, the ISS orbit and sensitivities to large zenith angle EASs allow the full coverage of the entire Celestial Sphere. Knowing nighttime duration along with locational dependence of the cloud coverage, the expected exposure distribution may be computed.

In Figure 5 the exposure distribution is shown on the Celestial Sphere for highest energy EASs. The unity corresponds to uniformity. The impact of the cloud is investigated from the TOVS database [14]. In this analysis, we assume the nadir mode and the cases with cloud-top altitudes lower than 3.2 km as fiducial regions.

The distribution of exposure is primarily determined by astronomical factors. In each latitude, the observable sky regions in declination are limited. The distribution in declination is a result of integration over latitudes within $\pm 51.6^\circ$ taking into account that the resident time of the ISS. The distribution in right ascension (RA) intrinsically has non-uniformity due to longer twilight around the time of solstices although the effect is not dramatic as seen in ground-based observatories. This results in deficits around 6 h and 18 h in RA.

Another factor is due to global cloud distribution and its seasonal variation. In the present work, we assume the clear atmosphere and clouds at low altitudes that allows visibility of the EAS maximum for $\Theta > 30^\circ$. Favorable scenes are found in dry land and ocean in part. On the contrary, there are less efficient areas near Equator like rainforest. The figure shows the summary of overall effects. In first one-year operation, the entire Celestial Sphere is completely observed with a $\pm 10\%$ uniformity.

6 Summary and outlook

In the present work, we discuss an overview of the JEM-EUSO performance focusing on the expected exposure. Generating a large number of EAS events by the ESAF package, one-year operation for $H_0 = 400$ km in the nadir mode results in about 9-year exposures by Auger at highest energies. With subsection of the aperture, annual exposure similar to larger than that of the Auger is achieved at energies $\sim (3-4) \times 10^{19}$ eV. This allows cross-check with those data. The performance in quasi-nadir and tilt modes are also considered. The former effectively allows a recovery of the observation area in case of lower altitude operation and the latter enhances exposures at highest energies. Thanks to the ISS orbit, the all-sky survey with the JEM-EUSO telescope alone is achievable at high degree of uniformity. This is a distinct feature compared with ground-based observatories and significantly reduces uncertainties in source search efforts.

The scope of the present work focuses on the trigger, while the performance in reconstruction and the role of the AM system are discussed in Refs [4, 12]. The aperture and exposure herein are derived with specific assumptions on the detector properties, background level, EAS development etc. Recent introduction of the JEM-EUSO configuration into the Offline code [15] will systematically allow cross-checks in simulation processes.

Acknowledgment

The present work has been partly supported by the ESA Topical Team Activities Fund and by the DLR, Deutsches Zentrum für Luft- und Raumfahrt, Germany, by the Italian Ministry of Foreign Affairs General Direction for the Cultural Promotion and Cooperation and by Slovak Academy of Sciences MVTS JEM-EUSO as well as VEGA grant agency project 2/0081/10. The computing facility of RICC (RIKEN Integrated Cluster of Clusters) has been used for the simulation study.

References

[1] For review, Letessier-Selvon, A. and Stanev, T., Rev. Mod. Phys. 83, 907 (2011).
[2] Takahashi, Y. and JEM-EUSO Collaboration, New J. Phys. 11, 065009/1-21 (2009); Santangelo, A. et al., these Proc. #738 (2013).
[3] Medina Tanco, G. et al., these Proc. #937 (2013).
[4] Neronov, A. et al., these Proc. #1072 (2013); Morales de los Rios, J.A. et al., these Proc. #514 (2013).
[5] NASA, *ISS User's Guide-Release 2.0* (2000); JAXA Human Space Systems and Utilization Program Group, *Kibo Handbook* (2007).
[6] Takizawa, Y. et al., these Proc. #832 (2013).
[7] Kajino, F. et al., these Proc. #1128 (2013).
[8] Catalano, O. et al., Proc. 31st ICRC, Lodz, #0326 (2009); Bayer, J. et al., these Proc. (2013).
[9] B. Pastircak et al., these Proc. #754 (2013).
[10] Berat, C. et al., Astropart. Phys. 33, 211 (2010).
[11] Adams Jr., J.H. et al. Astropart. Phys. 44, 76 (2013).
[12] Mernik, T. et al. these Proc. #777 (2013).
[13] Estimated from www.auger.org
[14] TOVS (TIROS Operational Vertical Sounder), http://www.ozonelayer.noaa.gov/action/tovs.htm/
[15] Argiro, S. et al., Nucl. Instrum. Meth. A580, 1485 (2007).